International Journal of Microwave and Wireless Technologies

cambridge.org/mrf

A compact dual-band D-CRLH-based antenna with self-isolation functionality

Mahmoud A. Abdalla[1], Mohamed El Atrash[2], Ahmed A. Abdel Aziz[1] and Mohamed I. Abdelnaser[1]

[1]Electronic Engineering Department, Military Technical College Cairo, Cairo, Egypt and [2]Electrical Systems Engineering Department, October University for Modern Sciences and Arts, Giza, Egypt

Research Paper

Cite this article: Abdalla MA, El Atrash M, Abdel Aziz AA, Abdelnaser MI (2022). A compact dual-band D-CRLH-based antenna with self-isolation functionality. *International Journal of Microwave and Wireless Technologies* **14**, 616–625. https://doi.org/10.1017/S1759078721000738

Received: 31 December 2020
Revised: 22 April 2021
Accepted: 23 April 2021
First published online: 14 May 2021

Keywords:
D-CRLH; metamaterial; multi-band antenna; negative refractive index; self-filtering

Author for correspondence:
Mahmoud A. Abdalla,
E-mail: maaabdalla@ieee.org

Abstract

This paper presents a compact dual-band filtering antenna without extra employing of filter structures. The antenna is designed using a planar dual-composite right/left-handed (D-CRLH) transmission line unit cell, where the filtering function is achieved through current cancellation between the D-CRLH resonators. The antenna is designed to function at 3.0 and 5.1 GHz, which can serve different WLAN applications. The antenna is a co-planar waveguide fed with a very compact size of only $30 \times 16\ mm^2$. Compared to the conventional patch antenna, the antenna size is only 17% at 3.0 GHz and 31% at 5.1 GHz. Despite the small size, the antenna preserves a good omni-directional radiation pattern at the two resonant frequencies with a measured realized gain of 2 and 2.7 dB, respectively. At the stopband in-between the two resonant bands, the reflection coefficient is almost 0 dB at 4.25 GHz and complete non-radiation is proved with a −11 dB measured realized gain. The different antenna filtering functions are verified by full-wave simulation and measurements.

Introduction

With the development of hand-held devices, it is a necessity that front-end wireless system components and antennas possess compactness and multi-resonance functionality. This is due to the fact that they contribute to the overall system size miniaturization [1, 2]. Numerous miniaturization methodologies have been applied in the literature to reduce the antenna design footprint. In [3, 4], the antennas were designed using the concept of folding/meandering to fill the whole space. Loading of reactive termination (inductive/capacitive), resulting in a slow-wave structure, increased the propagation constant; hence, the antenna looks electrically longer [5, 6]. However, this approach increases the quality factor leading to narrow bandwidth antennas. Another technique was proposed in [7, 8], which included loading the radiator elements with dielectric/magnetic elements or combinations of them. Moreover, loading the antenna with parasitic elements and fractal shape reflectors can attain size reduction, as was proposed in [9]. Furthermore, loading the antenna ground planes with resonators; such as, defected ground structure, can support size reduction [10], but this increases the back radiation of the antenna.

Based on theory, electrical small antennas require their size to validate condition $ka < 1$, where "a" is the minimum sphere radius that circumscribes the antenna. This condition is reduced to half if the antenna is mounted on a perfect ground plane ($ka < 0.5$) [11–14]. Thus, for all the previous designs, to maintain good antenna performance, the designers should consider the fundamental limit of antenna small size. Otherwise, the antenna bandwidth, gain, and efficiency may exhibit severe degradation.

Multi-band function in antennas is another advantage requirement. There are many techniques that have been proposed for attaining multi-band resonances. Examples for these approaches may include (1) meandering the monopole [15], (2) incorporating various defecting ground radiating resonators [16]; yet, it may increase the antenna size, (3) loading the monopole with slots and stubs to accomplish additional resonances [17, 18], (4) integrating the monopole antenna with artificially engineered material-based resonators [19–21]. Among the different metamaterial's configurations, the planar composite right/left-handed (CRLH) planar transmission line [22, 23] and its dual form [24] are very attractive for achieving small and multi-band resonant antennas. These are mainly achieved due to the possible design of arbitrary value/frequency non-linear propagation constant.

When it comes to designing compact and multi-band antennas, the filtering/isolation in-between the operating bands should be considered, especially for the nearby resonant frequencies. One approach is to cascade the antenna with a bandstop filter [25–28]. Nevertheless, this concept results in an increase in the antenna footprint, which is not desired. As such, it is preferable that the antenna possesses self-filtering properties to maintain the compact size specification [29–37]. In [38], a dual-band filtering antenna, operated by exciting two orthogonal modes, was presented. It was shown in [39] that wide-band filtering antennas can be achieved

© The Author(s), 2021. Published by Cambridge University Press in association with the European Microwave Association

by loading bandstop filters. In [40], the utilization of coupled split-ring resonator cells was presented to attain a monopole antenna that holds high efficiency, dual-band resonances with wide bandwidths, in addition to self-isolation functionalities. The dual-CRLH (D-CRLH) transmission line is characterized by selective filtering response and was incorporated in selective microwave resonators, filters, diplexers [41, 42] and filtering antennas [43] with only conceptual analysis.

Proposed in this paper is an inspired D-CRLH monopole antenna that is compact in size, exhibits dual-band resonances, and displays self-filtering characteristics that might enable it to be realized in WiMAX applications. Presented in section "D-CRLH unit cell" are the thorough steps for designing and characterizing the D-CRLH cell. Highlighted in section "D-CRLH antenna results and analysis" are the D-CRLH antenna design concepts, full-wave simulations, and experimental measurements.

D-CRLH unit cell

D-CRLH unit-cell analysis

The proposed antenna is designed based on a D-CRLH unit cell. The dispersion propagation coefficient (β) along D-CRLH TL can be extracted by applying the periodic analysis of the infinite number of cells of length (d) as [24]

$$\cos(\beta d) = \cos(\theta) + \frac{1}{2} Z Y \cos^2\left(\frac{\theta}{2}\right) + i \frac{1}{2}(Z_o Z + Y_o Y) \sin\left(\frac{\theta}{2}\right), \quad (1)$$

where θ is the hosting transmission line electrical length, Z_0 and Y_0 are the right-handed characteristic impedance and admittance, respectively. An example of dispersion diagram of D-CRLH transmission line is given in Fig. 1(a) where it demonstrates two passbands separated with a sharp stopband in between.

The equivalent circuit of the realized D-CRLH cell is shown in Fig. 1(b). In the equivalent circuit, the elements L_R, L_L, C_R, and C_L are representing the distributed loading elements of the hosting microstrip transmission line. To account for any patristic elements of the hosting transmission line that may exist, the elements (L_{par} and C_{par}) are introduced. Also, the inductor L_{PC} represents the series parasitic inductance of the employed distributed capacitor (C_L).

Following the above-discussed equivalent circuit then, the total equivalent series impedance Z, and shunt admittance Y are found to be as follows:

$$Z = Z_1 + \frac{Z_2 Z_3}{Z_2 + Z_3}, \; Z_1 = j\omega L_{par} \text{ and } Z_2 = j\omega L_R \text{ and } Z_3 = j\omega L_{CP} + \frac{1}{j\omega C_L}, \quad (2)$$

$$Y = Y_1 + Y_2 \text{ and } Y_1 = j\omega C_{Par} \text{ and } Y_2 = \frac{1}{j\omega L_L + 1/j\omega C_R}. \quad (3)$$

To calculate the cut-off frequencies for the D-CRLH cell and assuming small hosting line length ($\theta \to 0$), βd in equation (1) should have either π or zero. Then satisfying with equations (2) and (3), equation (1) will be

$$\left(j\omega L_{Par} + \frac{j\,\omega\, L_R\,(1 - \omega^2\, L_{cp}\, C_L)}{(1 - \omega^2\,(L_{cp} + L_R)\, C_L)}\right) \times \left(\frac{j\,\omega\,(C_R + C_{par}) - j\,\omega^3\, C_{par}\, C_R\, L_L}{1 - \omega^2\, L_L C_R}\right) = A, \quad (4)$$

where A is a constant = (−4) or (0) for $\beta d = \pi$ or $\beta d = 0$, respectively. The condition $\beta d = \pi$ yields the cut-off frequencies (f_{c1} and f_{c2}) whereas the condition, $\beta d = 0$, the lower (f_{c0}) and upper cut-off frequency (f_{c3}) and (f_{c4}) in Fig. 1. For example, for $\beta d = 0$, the cut-off frequencies can be calculated as

$$Z = 0 \Rightarrow f_{c3} = \frac{1}{2\pi}\sqrt{\frac{L_R + L_{par}}{C_L\,(L_R L_{CP} + L_{par}\,(L_R + L_{CP}))}}, \quad (5a)$$

$$Y = 0 \Rightarrow f_{c4} = \frac{1}{2\pi}\sqrt{\frac{1 + C_{par}/C_R}{C_{par}\, L_L}}. \quad (5b)$$

The characteristic impedance for the D-CRLH will be employed in the matching process as

$$Z_{\text{DCRLH}} = \sqrt{\frac{Z}{Y}} = \sqrt{\left(j\omega L_{par} + \frac{j\,\omega\, L_R\,(1 - \omega^2\, L_{cp}\, C_L)}{(1 - \omega^2\,(L_{cp} + L_R)\, C_L)}\right) \Big/ \left(\frac{j\,\omega\,(C_R + C_{par}) - j\,\omega^3\, C_{par}\, C_R\, L_L}{1 - \omega^2\, L_L C_R}\right)}. \quad (6)$$

From (6) it can be concluded that the D-CRLH TL does not have constant impedance over the propagation bands. The propagation constant profile in (1) is a non-linear function. Neglecting the effect of parasitic elements (L_{par}, L_{PC}, C_{par}), the definition for the propagation constant in equation (1) may be further simplified for a short length of hosting transmission line to be as in (7)

$$\beta d = \omega\sqrt{\frac{L_R C_R}{(1 - \omega^2 L_R C_L)\,(1 - \omega^2 C_R L_L)}} = n\pi, \; n = 0, \pm 1, \pm 2, .. \quad (7)$$

Moreover, it is clear that the cut-off frequencies, characteristic impedance, and progressive phase shift are controlled by the values of the loading elements. This will be emphasized in the following sub-section.

Initial design

To meet the final proposal, filtering D-CRLH cell is designed to have passbands at 3 and 5.1 GHz with stopband between the

https://doi.org/10.1017/S1759078721000738 Published online by Cambridge University Press

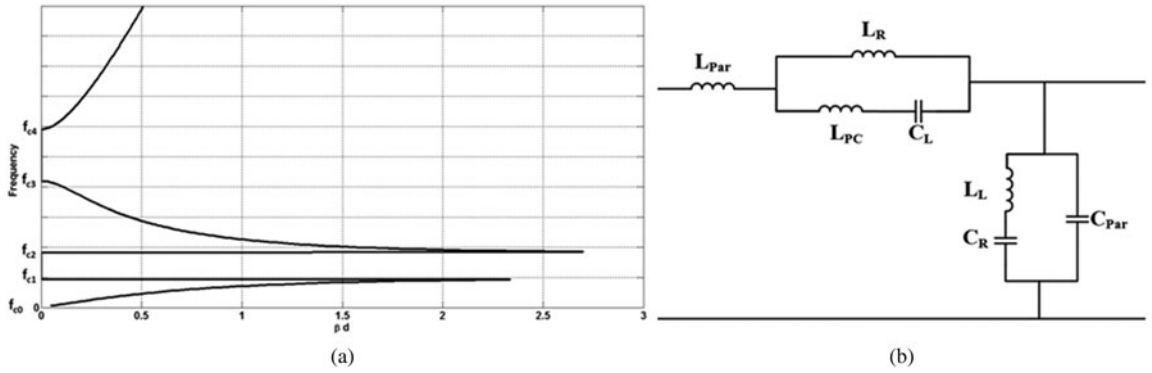


Fig. 1. (a) The dispersion diagram of an unbalanced D-CRLH transmission line. (b) The equivalent circuit model for a general D-CRLH unit.

two passbands, at 4.1–4.8 GHz. This is applied to design a dual-band self-filtering antenna serving WLAN applications. The equivalent circuit element values that fulfil the desired frequency bands are found to be; $L_{par} = 1.2$, $L_{PC} = 2.335$, $L_L = 4.804$, $L_R = 2.0874$ (all in nH), $C_L = 0.2942$, $C_R = 0.1.2872$, $C_{par} = 0.8$ (all in pF). The calculated equivalent circuit is simulated using ADS (Advanced Design System) with the results shown in Fig. 2.

The designed equivalent cell elements are translated to 3D design. Rogers RO4350 substrate with 0.813 mm thickness is selected as a hosting material with coplanar waveguide (CPW) configuration for the cell. As shown in Fig. 3, the D-CRLH cell is realized with a parallel tank circuit formed with a six-finger interdigital capacitor and one series strip inductance. This is represented by the lumped elements L_R and C_L in Fig. 1(b). Similarly, the thin transmission line's length (L_{L_SH}) and width (W_{L_SH}) are connected to a parallel plate capacitor (L_p) on one side of the CPW grounds. It is worth noting that the green color denotes the metallic cell, while the grey color represents the substrate. This proposed geometry was suggested to achieve high gain for the antenna. These elements are corresponding to the lumped components C_R, and L_L in Fig. 1(b).

All equivalent elements are translated to 3D structures based on [44]. The realized 3D cell is shown in Fig. 3 with detailed dimensions shown in Table 1. The cell is simulated using CST simulation tool and the simulation results are compared to equivalent circuit simulation as in Fig. 2. As shown, there is a passband from around 2.6 to 3.7 GHz and from 4.9 to above 5.9 GHz. The two passbands are separated with a stopband with ranges from 4.1 to 4.8 GHz, insuring filtering specification of the cell. The EM simulation results are compared with the equivalent circuit simulation with a high agreement between them.

To ensure the correct design steps, the phase of the transmission coefficient (S_{21}) for both EM and circuit simulations is shown in Fig. 4(a). As shown, the deigned cell has −180 degree at 3 GHz and 180 degree at 5.1 GHz of the transmission coefficient phases for circuit simulations and EM simulations. Finally, the dispersion diagram of the designed filtering cell based on EM simulations is shown in Fig. 4(b). As shown, the dispersion diagram result agree with the magnitude and the phase results of the transmission coefficient as shown in Figs 3 and 4(a), respectively.

D-CRLH antenna results and analysis

The unit cell discussed in the previous sub-section is modified to the antenna shown in Fig. 5(a), and simulated. The 2D layout of

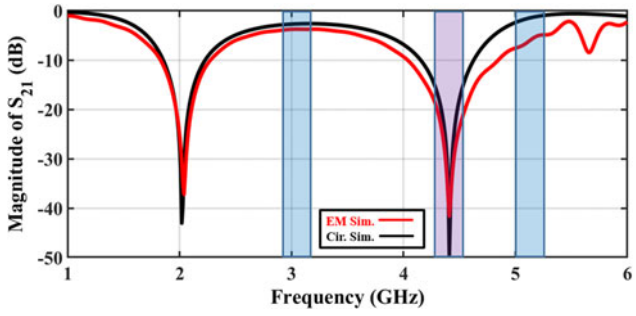


Fig. 2. Comparison between the equivalent circuit and EM simulation results for the transmission coefficient (S_{21}) magnitude.

the proposed antenna is shown in Fig. 3. The detailed dimensions are as that used in Table 1, with some minor modification to optimize the antenna results. The fabricated antenna prototype is shown in Fig. 5(b). It is worth noting that the green color denotes the metallic radiator, while the grey color represents the substrate.

The dual-band D-CRLH antenna results

The simulated and measured reflection coefficients of the designed D-CRLH antenna are shown in Fig. 6. As noticed, the prototype exhibits dual-band resonances along with the stopband in-between the resonant bands. The simulated first band ranges from 2.8 to 3.2 GHz (fractional bandwidth of 13.33%) and has a center frequency at 3.0 GHz, at which the reflection coefficient is −22 dB. The measured one is wider and extends from 2.73 to 3.7 GHz (fractional bandwidth of 32.33%) with the center frequency at 3.0 GHz, at which the reflection coefficient is −44 dB.

On the other hand, the simulated second band ranges from 4.9 to 5.2 GHz (fractional bandwidth of 6%) and has a center frequency at 5.1 GHz, at which the reflection coefficient is −11.4 dB. The measured one is slightly wider and extends from 4.9 to 5.4 GHz (fractional bandwidth of 9.8%) and has a center frequency at 5.1 GHz with the reflection coefficient of −16 dB. Hence, the simulated and measured results confirm the first and second band center frequencies at 3.0 and 5.1 GHz, respectively. Such discrepancies between the simulated and measured results may be claimed due to the fabrication resolution accuracy.

The stopband center frequency, possessing maximum isolation, occurs at 4.25 GHz, which is indicated by the fact that the

https://doi.org/10.1017/S1759078721000738 Published online by Cambridge University Press

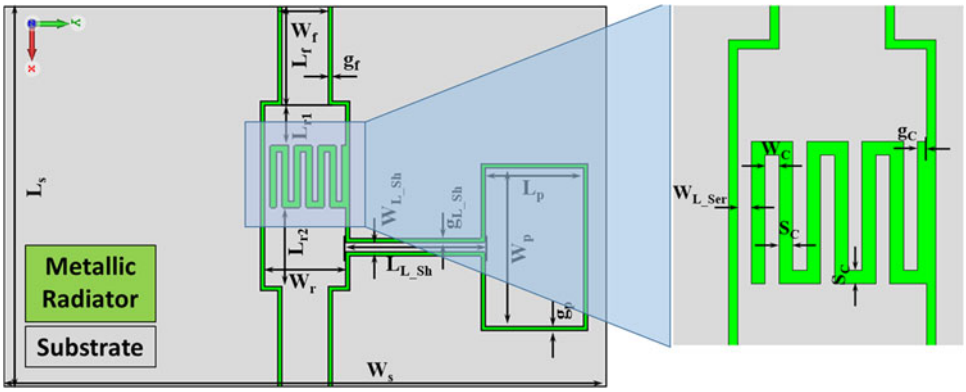


Fig. 3. The realized 2D shape of the D-CRLH unit cell.

Table 1. The detailed dimensions for the unit-cell

Par.	Dim.	Par.	Dim.	Par.	Dim.	Par.	Dim.
W_s	30	L_{r1}	2	W_p	5	W_C	0.3
L_s	19	L_{r2}	4	L_{L_Sh}	7	S_C	0.3
W_f	2.3	W_r	4.1	W_{L_Sh}	0.5	W_{L_Ser}	0.3
L_f	5	L_p	8	g_{L_Sh}	0.2		
g_f	0.2	g_p	0.2	g_c	0.2		

All design parameters are in mm.

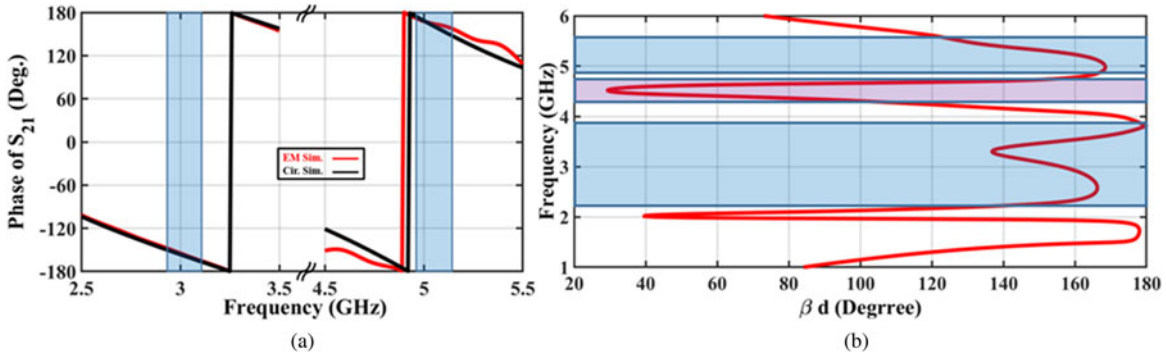


Fig. 4. (a) Comparison between the equivalent circuit and EM simulation results for the phase of transmission coefficient. (b) The dispersion diagram of the proposed D-CRLH unit cell.

reflection coefficient is almost 0 dB. Furthermore, the −3 dB bandwidth covers from 3.7 to 4.52 GHz.

Comparing the antenna size, at the two resonant frequencies, to a conventional patch antenna, it can be determined that the conventional patch antenna footprint is 62×48 mm^2 and 42.4×36.4 mm^2 at 3.0 and 5.1 GHz, respectively. Hence, the proposed antenna has a very small size which is only 17% at 3.0 GHz and 31% at 5.1 GHz when benchmarked against the conventional patch antenna.

The performance analysis of the designed antenna can be understood by demonstrating the surface current distribution at the resonant frequencies for the same current levels. These simulated results are plotted in Figs 7(a) and 7(b) at 3.0 and 5.1 GHz, respectively. It can be observed that the current is concentrated around the series branch than the shunt branch at 3.0 GHz. However, at 5.1 GHz, the current starts to increase and focus in the shunt branch in comparison to the series branch, as depicted in Figs 7(a) and 7(b), respectively. Furthermore, to confirm the good stopband in-between the two operating bands, the surface current distribution at 4.25 GHz is plotted in Fig. 8, for the same current levels as those in Fig. 7. It can be observed that the current, at the two resonators, follows a complete rotation cycle, which in radiation calculation cancel-out one other. The currents flow in opposite directions; thus, they result in a total bandstop filtering outcome. This observation confirms the almost 0 dB reflection coefficient, signifying total reflection, at that frequency, as was observed in Fig. 6.

The antenna radiation properties

The radiation and filtering properties of the proposed antenna have been emphasized in two main steps. The first one is by

https://doi.org/10.1017/S1759078721000738 Published online by Cambridge University Press

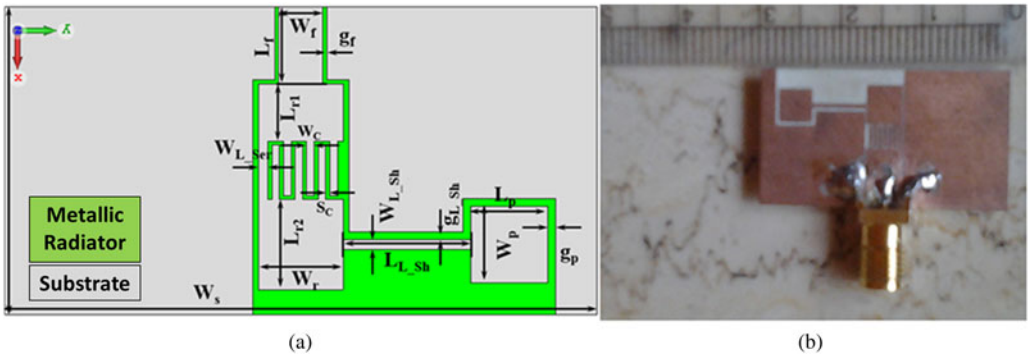


Fig. 5. (a) The 2D layout of the dual-band D-CRLH antenna. (b) The fabricated D-CRLH antenna.

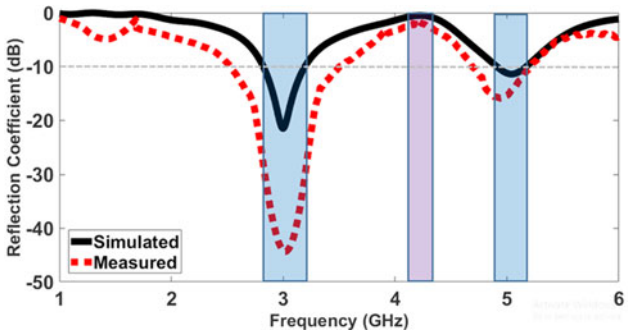


Fig. 6. The simulated and measured reflection coefficients of the dual-band D-CRLH antenna.

depicting the maximum antenna realized gain and antenna total efficiency as a function of frequency, as shown in Figs 9 and 10, respectively. Moreover, tabulated in Table 2 are the simulated and measured realized gains and total efficiencies at the two resonant center frequencies and the stopband mid-frequency.

Now, observing Fig. 9, it is evident that the simulated and measured realized gains highly agree, where the proposed antenna achieves good realized gain of 2 and 2.7 dB at 3.0 and 5.1 GHz, respectively, despite its highly compact size.

Moreover, the proposed antenna measured total efficiency agrees with the simulated one in the low resonant frequency, as portrayed in Fig. 10. However, there is a considerable discrepancy between both efficiency outcomes in the high resonant band.

It is worth to comment that the antenna reflection efficiency $e_r = 10 \log (1-|S_{11}|^2)$ can be calculated from Fig. 6 as follows. At 3 GHz, simulated S_{11} is −11 dB and hence $e_r = 92\% = -0.36$ dB and at 5.1 GHz, S_{11} is −21 dB and hence $e_r = 99\% = -0.034$ dB. Also, without considering the reflection efficiency, the simulated antenna gain values were 2.26 dB at 3 GHz and 3.2 dB at 5.1 GHz. So, this gain increase compensates the difference in reflection efficiency so that the realized gain and total efficiency are almost identical as in Figs 9 and 10, respectively.

In addition, to further justify the stopband at 4.25 GHz, the proposed antenna displayed very low gain and total efficiency values, whether simulated or measured. At 4.25 GHz, it exhibited simulated and measured realized gain values of −11 and −10 dB, respectively, as tabulated in Table 2, demonstrating no radiation. Furthermore, it exhibited simulated and measured total efficiency outcomes of 3.2 and 4.5%, respectively, as tabulated in Table 2.

Illustrated in Fig. 11 is the setup for measuring the proposed antenna normalized gain radiation pattern. Near-field measurements were conducted, where the StarLab Antenna Measurement – MVG was incorporated.

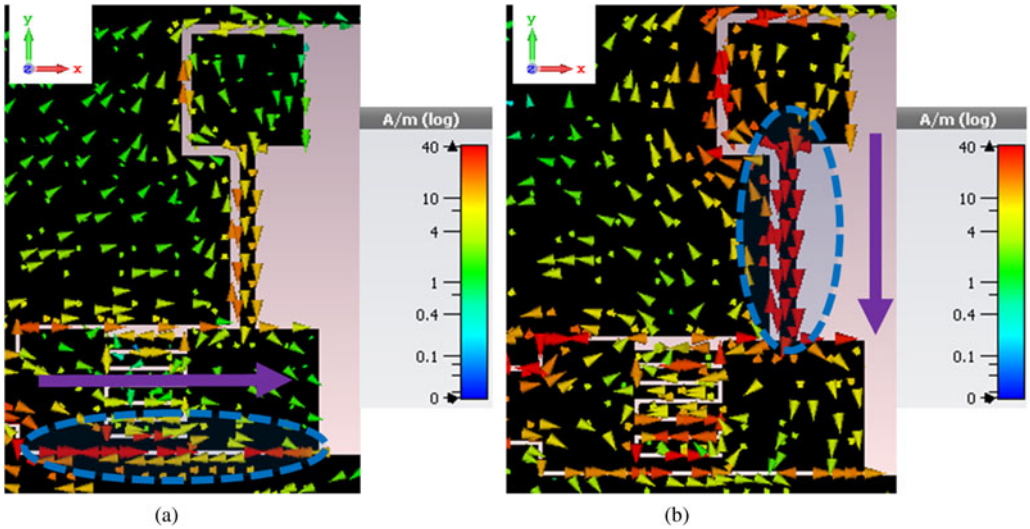


Fig. 7. The current distribution of the DCRLH antenna at (a) 3.0 GHz, (b) 5.1 GHz.

https://doi.org/10.1017/S1759078721000738 Published online by Cambridge University Press

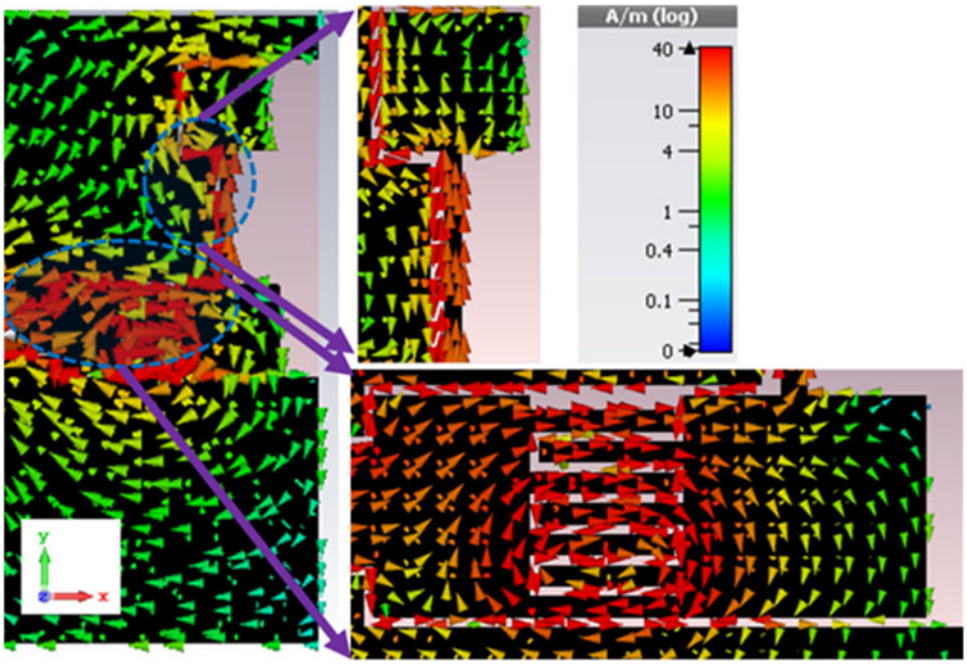


Fig. 8. The current distribution of the D-CRLH antenna at 4.25 GHz, indicating no radiation due to cancellation of currents.

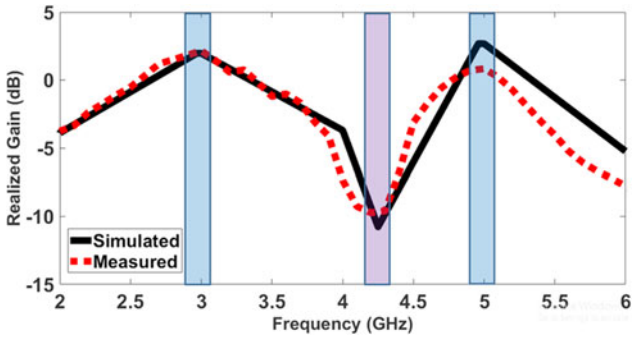


Fig. 9. Comparison between simulated and measured realized gain of the D-CRLH antenna.

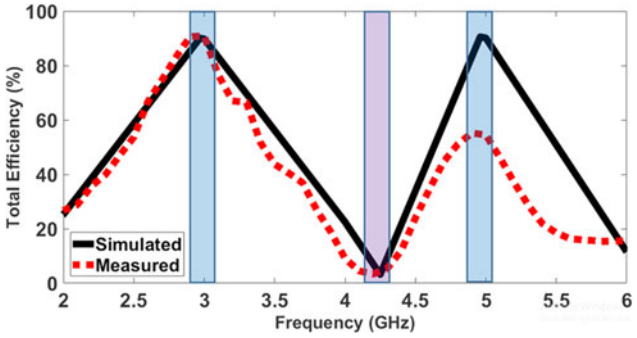


Fig. 10. Comparison between simulated and measured total efficiency of the D-CRLH antenna.

Table 2. The proposed D-CRLH antenna simulated and measured realized gain and total efficiency

Frequency (GHz)	Sim./meas. realized gain (dB)	Sim./meas. total effic. (%)
3.0	2/2	90.1/88
4.25	−11/−10	3.2/4.5
5.1	2.7/1	90.6/58



Fig. 11. Setup for the D-CRLH antenna radiation pattern measurement.

Displayed in Fig. 12 are the normalized polar plots of the gain radiation pattern at both resonant frequencies in the principal planes, where the *E*-plane denotes the *XZ*-plane (∅ = 0°), while the *H*-plane describes the *YZ*-plane (∅ = 90°). As portrayed in Figs 12(a) and 12(c), the antenna exhibits the figure-of-eight gain radiation pattern at both resonant frequencies in the *E*-plane, with a high agreement between the simulated and measured polar plots. Similarly, demonstrated in Figs 12(b) and 12(d)

https://doi.org/10.1017/S1759078721000738 Published online by Cambridge University Press

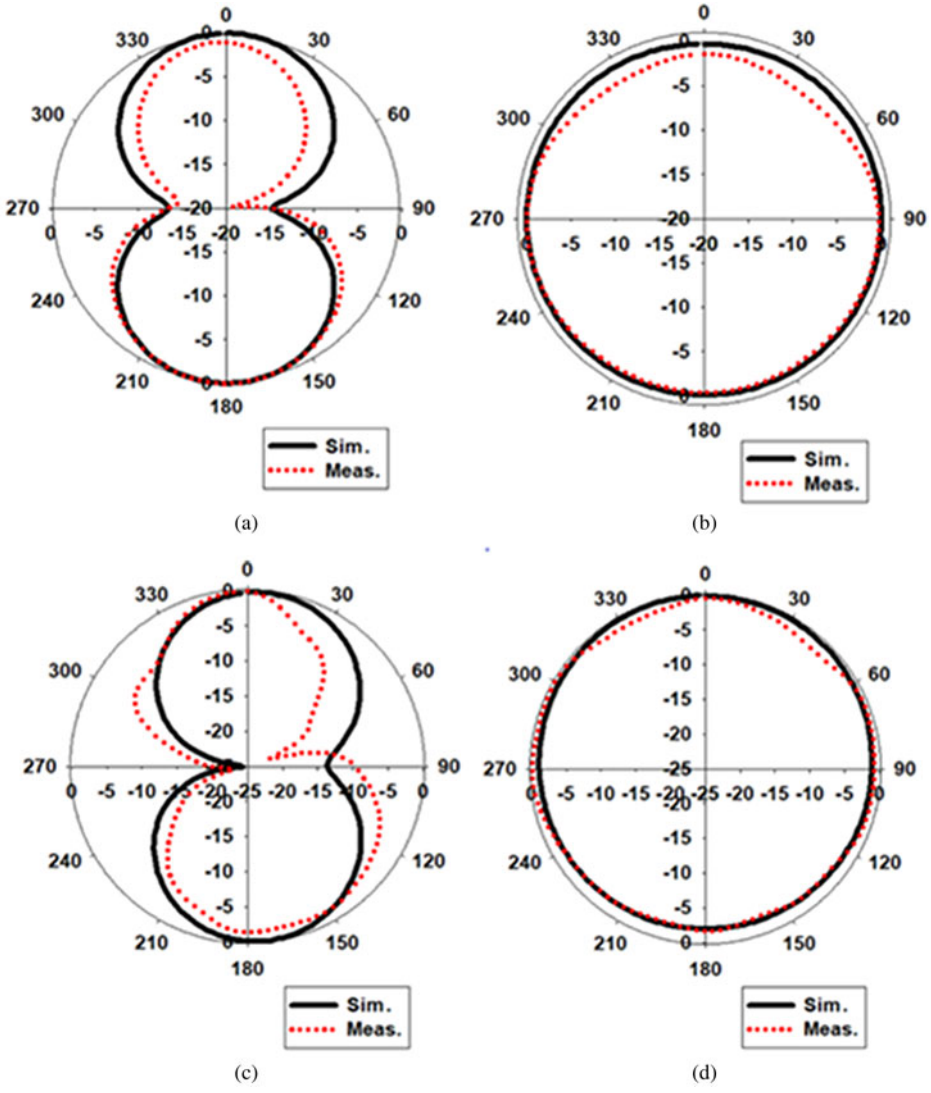


Fig. 12. Comparison between the simulated and measured normalized gain radiation patterns, in polar formats, in the principal planes at: (a) 3.0 GHz (*E*-plane); (b) 3.0 GHz (*H*-plane); (c) 5.1 GHz (*E*-plane); (d) 5.1 GHz (*H*-plane).

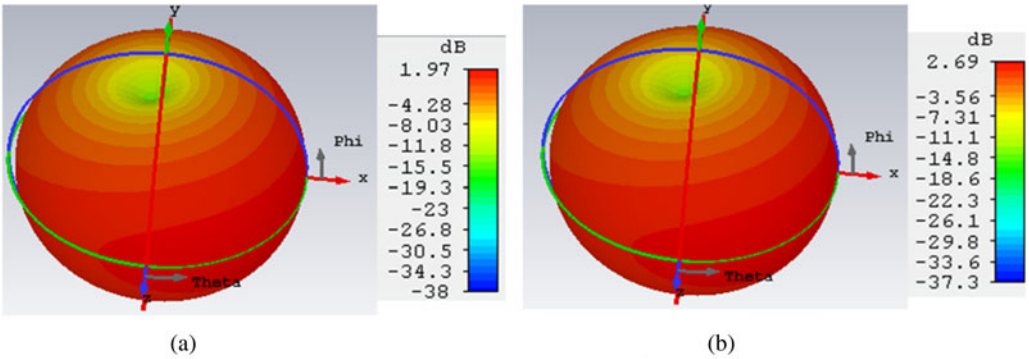


Fig. 13. The 3D gain radiation pattern of the D-CRLH antenna at (a) 3.0 GHz, (b) 5.1 GHz.

are the isotropic gain radiation patterns at 3.0 and 5.1 GHz, respectively, where it is clear that the simulated and measured polar plots highly agree. Hence, the antenna displays the omni-directional radiation pattern type. Next, the 3D gain radiation patterns at 3.0 and 5.1 GHz are portrayed in Figs 13(a) and 13(b), respectively. It is observed that the two radiation patterns are almost typical and exhibit the conventional omni-directional pattern with the same null direction along the *Y*-axis. This is due to the current cancellation witnessed along the CPW-ground planes.

https://doi.org/10.1017/S1759078721000738 Published online by Cambridge University Press

Table 3. Comparison between the proposed D-CRLH antenna and dual-band self-filtering antennas

Antenna/ publication year	Resonant frequency (GHz) bands	Realized gain (dB)/ total effic. (%)	Electrical size in terms of free-space wavelength (λ_0)	Measured max. S_{11} at bandstop center frequency (dB)
Proposed work	3 5.1	2/90 2.7/91	0.3 × 0.16 × 0.0085 at 3 GHz	−1
[33]/2018	2.6 3.45	8.4/N.A. 7.7/N.A.	0.43 × 0.43 × 0.26 at 2.6 GHz	N.A.
[34]/2018	4.3 5.02	5.94/N.A. 6.45/N.A.	0.129 × 0.129 × 0.0113 at 4.3 GHz	0
[35]/2019	9.5 10.5	5.75/N.A. 5.95/N.A.	0.697 × 0.697 × 0.05 at 9.5 GHz	−4
[36]/2018	2 3.5	1.56/N.A. 0.46/N.A.	0.272 × 0.169 × 0.0102 at 2 GHz	0
[38]/2016	1.9 2.6	6.7/N.A. 7.3/N.A.	0.51 × 0.633 × 0.01 at 1.9 GHz	0
[40]/2020	3 6	2.16/95 3.13/90	0.3 × 0.3 × 0.008 at 3 GHz	−1

The proposed D-CRLH antenna is benchmarked against other dual-band antennas holding the self-isolation feature, as tabulated in Table 3. The aspects at which comparison was conducted included the antennas resonant frequencies, the antenna electrical size with respect to the free-space wavelength, the peak value of the reflection coefficient at the stopband center frequency, the realized gain, and the total efficiency. It can be seen that the proposed antenna is highly compact and competes with the other references in terms of size. Moreover, it displays a better out-of-band suppression than [35], and almost the same as [34, 36, 38], and [40]. Finally, despite its low profile, it exhibits a good realized gain and total efficiency at the two resonant frequencies. Hence, the proposed D-CRLH antenna could be nominated for wireless communication applications.

Conclusion

This paper presents a compact dual-band metamaterial-based antenna for wireless applications at 3.0 and 5.1 GHz. The antenna is constructed using only one cell of a D-CRLH transmission line in a simple CPW configuration. The antenna electrical size is only $0.3\,\lambda_0 \times 0.16\,\lambda_0$ at the low resonant frequency. This is considered a very small size, which is only 17% at 3.0 GHz and 31% at 5.1 GHz, compared to a single-band conventional microstrip patch antenna. Moreover, the antenna displays the monopole-like radiation pattern type with a realized gain of 2 dB at 3.0 GHz and 2.7 dB at 5.1 GHz. Without the integration with a filtering structure, the antenna exhibits a stopband at the center frequency of 4.25 GHz with a realized gain of −11 dB. At 4.25 GHz, this is attained as a result of the current cancellation between the D-CRLH-based resonators. Based on the highly compact size and the presented results, the proposed antenna can serve WiMAX wireless devices.

References

1. **Wong K-L** (2004) *Compact and Broadband Microstrip Antennas*, vol. **168**. New Jersey, USA: John Wiley & Sons.
2. **Guha D and Antar YMM** (eds) (2011) *Microstrip and Printed Antennas: New Trends, Techniques and Applications*. New Jersey, USA: John Wiley & Sons.
3. **Makimura H, Watanabe Y, Watanabe K and Igarashi H** (2011) Evolutional design of small antennas for passive UHF-band RFID. *IEEE Transactions on Magnetics* **47**, 1510–1513.
4. **Medeiros CR, Costa JR and Fernandes CA** (2011) RFID reader antennas for tag detection in self-confined volumes at UHF. *IEEE Antennas and Propagation Magazine* **53**, 39–50.
5. **Chi PL, Waterhouse R and Itoh T** (2011) Antenna miniaturization using slow wave enhancement factor from loaded transmission line models. *IEEE Transactions on Antennas and Propagation* **59**, 48–57.
6. **Lai C-P, Chiu S-C and Chen S-Y** (2012) Miniaturization of CPW-fed slot antennas using reactive terminations and truncated bilateral ground plane. *IEEE Antennas and Wireless Propagation Letters* **11**, 1072–1075.
7. **Lee J, Lee J, Min K and Cheon Y** (2014) Miniaturized antennas with reduced hand effects in mobile phones using magneto-dielectric material. *IEEE Antennas and Wireless Propagation Letters* **13**, 935–938.
8. **Karilainen AO, Ikonen PMT, Simovski CR, Tretyakov SA, Lagarkov AN, Maklakov SA, Rozanov KN and Starostenko SN** (2011) Experimental studies on antenna miniaturization using magneto-dielectric and dielectric materials. *IET Microwaves, Antennas & Propagation* **5**, 495–502.
9. **Collins S and Antar YMM** (2004) Antenna size reduction using Yagi-Uda loops and shorted circular patches. *IEEE Transactions on Antennas and Propagation* **52**, 855–864.
10. **Kimouche H and Oukil S** (2012) Electrically small antenna with defected ground structure, In 2012 42nd European Microwave Conference, 811–814.
11. **Wheeler HA** (1947) Fundamental limitations of small antennas. *Proceedings of the IRE* **35**, 1479–1484.
12. **McLean JS** (1996) A re-examination of the fundamental limits on the radiation Q of electrically small antennas. *IEEE Transactions on Antennas and Propagation* **44**, 672–676.
13. **Geyi W** (2003) Physical limitations of antenna. *IEEE Transactions on Antennas and Propagation* **51**, 2116–2123.
14. **Davis WA, Yang T, Caswell ED and Stutzman WL** (2011) Fundamental limits on antenna size: a new limit. *IET Microwaves, Antennas & Propagation* **5**, 1297–1302.
15. **Park Y, Kang D and Sung Y** (2012) Compact folded triband monopole antenna for USB dongle applications. *IEEE Antennas and Wireless Propagation Letters* **11**, 228–231.
16. **Liu W, Wu C and Dai Y** (2017) Design of triple-frequency microstrip-fed monopole antenna using defected ground structure. *IEEE Transactions on Antennas and Propagation* **59**, 2457–2463.
17. **Moosazadeh M and Kharkovsky S** (2014) Compact and small planar monopole antenna with symmetrical L- and U-shaped slots for WLAN/WiMAX applications. *IEEE Antennas and Wireless Propagation Letters* **13**, 388–391.

https://doi.org/10.1017/S1759078721000738 Published online by Cambridge University Press

18. **Lu W-J, Zhu L, Tam KW and Zhu H-B** (2017) Wideband dipole antenna using multi-mode resonance concept. *International Journal of Microwave and Wireless Technologies* **9**, 365–371.
19. **Da Xu K, Li D, Liu Y and Liu QH** (2018) Printed quasi-Yagi antennas using double dipoles and stub-loaded technique for multi-band and broadband applications. *IEEE Access* **6**, 31695–31702.
20. **Ntaikos DK, Bourgis NK and Yioultsis TV** (2011) Metamaterial-based electrically small multiband planar monopole antennas. *IEEE Antennas and Wireless Propagation Letters* **10**, 963–966.
21. **Reddy SV, Sarkar D, Saurav K and Srivastava KV** (2015) A compact CRLH unit cell loaded triple-band monopole antenna. *Microwave and Optical Technology Letters* **57**, 115–119.
22. **Caloz C and Itoh T** (2006) *Electromagnetic Metamaterials Transmission Line Theory and Microwave Applications*. New Jersey: J. Wiley & Sons.
23. **Ghosh K and Das S** (2020) Circularly polarized ACPW Fed CRLH-TL based ZOR antenna with band notch characteristics. *International Journal of Microwave and Wireless Technologies* **12**, 387–397.
24. **Caloz C** (2006) Dual composite right/left-handed (D-CRLH) transmission line metamaterial. *IEEE Microwave and Wireless Components Letters* **16**, 585–587.
25. **Abdalla MA and Fouad A** (2016) Integrated filtering antenna based on D-CRLH transmission lines for ultra-compact wireless applications. *Progress In Electromagnetics Research C* **66**, 29–38.
26. **Mao CX, Gao S, Wang Y, Wang Z, Qin F, Izquierdo BS and Chu QX** (2016) An integrated filtering antenna array with high selectivity and harmonics suppression. *IEEE Transactions on Microwave Theory and Techniques* **64**, 1798–1805.
27. **Jiang ZH, Gregory MD and Werner DH** (2016) Design and experimental investigation of a compact circularly polarized integrated filtering antenna for wearable biotelemetric devices. *IEEE Transactions on Biomedical Circuits and Systems* **10**, 328–338.
28. **Masoodi IS, Ishteyaq I, Muzaffar K and Magray MI** (2020) A compact band-notched antenna with high isolation for UWB MIMO applications. *International Journal of Microwave and Wireless Technologies*, 1–7.
29. **Abdalla MA** (2017) A high selective filtering small size/dual band antenna using hybrid terminated modified CRLH cell. *Microwave and Optical Technology Letters* **59**, 1680–1686.
30. **Abdalla M, Karimian S and Hu Z** (2014) Dual band spurious-free SIR metamaterial antenna, In 2014 IEEE International Antennas & Propagation Symposium Digest, 1005–1006.
31. **Yu C, Hong W, Kuai Z and Wang H** (2012) Ku-band linearly polarized omnidirectional planar filtenna. *IEEE Antennas and Wireless Propagation Letters* **11**, 310–313.
32. **Deng J, Hou S, Zhao L and Guo L** (2018) A reconfigurable filtering antenna with integrated bandpass filters for UWB/WLAN applications. *IEEE Transactions on Antennas and Propagation* **66**, 401–404.
33. **Liu Y, Wang S, Li N, Wang J-B and Zhao J** (2018) A compact dual-band dual-polarized antenna with filtering structures for sub-6 GHz base station applications. *IEEE Antennas and Wireless Propagation Letters* **17**, 1764–1768.
34. **Dhwaj K, Tian H and Itoh T** (2018) Low-profile dual-band filtering antenna using common planar cavity. *IEEE Antennas and Wireless Propagation Letters* **17**, 1081–1084.
35. **Khan AA and Mandal MK** (2019) Compact self-diplexing antenna using dual-mode SIW square cavity. *IEEE Antennas and Wireless Propagation Letters* **18**, 343–347.
36. **Hu P, Pan Y, Wa K and Zhang X** (2018) Wide-/dual-band omnidirectional filtering dielectric resonator antennas. *IEEE Transactions on Antennas and Propagation* **66**, 2622–2627.
37. **Vyas K and Yadav RP** (2020) Planar suspended line technique based UWB-MIMO antenna having dual-band notching characteristics. *International Journal of Microwave and Wireless Technologies*, 1–10.
38. **Zhang XY, Zhang Y, Pan Y-M and Duan W** (2016) Low-profile dual-band filtering patch antenna and its application to LTE MIMO system. *IEEE Transactions on Antennas and Propagation* **65**, 103–113.
39. **Tang M-C, Li C and Chen Y** (2020) Electrically small, planar, wideband filtering antenna with dual ring patches. *Electronics Letters* **56**, 61–62.
40. **Abdalla MA, El Atrash M, El-Sobky NA and Zahran SR** (2021) Concept and analysis of a coupled split ring resonator for wide-/dual bands, self-filtering, high out-of-band suppression and highly efficient antennas. *International Journal of Microwave and Wireless Technologies* **13**, 126–136.
41. **Choudhary DK, Abdalla MA and Chaudhary RK** (2019) Compact D-CRLH resonator for low pass filter with wide rejection band, high roll-off and transmission zeros. *International Journal of Microwave and Wireless Technologies* **11**, 509–516.
42. **Posadas VG, Martín JLJ, Cerrada AP, Munıoz LEG and Vargas DS** (2010) Dual-composite right-left-handed transmission lines for the design of compact diplexers. *IET Microwaves, Antennas & Propagation* **4**, 982–990.
43. **Abdalla MA and Abdelnaser MI** (2016) A compact dual band D-CRLH antenna with radiation pattern directional characteristics, In 2016 IEEE AP-S International Antenna and Propagation Symposium Digest, 277–278.
44. **Simons R and Simons RN** (2001) *Coplanar Waveguide Circuits, Components, and Systems*, Vol. **15**. New York: John Wiley.



Mahmoud A. Abdalla was born in 1973. He received the B.Sc. degree, with a grade of excellent with honors, in electrical engineering from the Electrical Engineering Department, Military Technical College, Cairo, Egypt in 1995. He was awarded the M.Sc. degree in electrical engineering from Military Technical College in 2000, and the Ph.D. degree from microwave and communication group, School of Electrical Engineering, Manchester University, UK, in 2009. He has been with Military Technical College since 1996 where he is a professor and leading the electromagnetic waves group in Electronic Engineering Department. Also, he is a visiting professor in the Department of Computer and Electrical Engineering, University of Waterloo, Canada since 2017. His research has focused on different metamaterial applications in microwave and millimeter bands, especially microwave components, miniaturized multi-band antennas, and ferrite components. Also, his research includes electromagnetic energy harvesting systems, EBG components, adaptive antenna systems for DOA estimation and interference cancellations, and radar absorber designs. He has published more than 200 peer-reviewed journal and conference papers. Dr. Abdalla is currently an IEEE senior member, URSI senior member, and a member of the IEEE and the European Microwave Association EuMA. He is an editorial member and reviewer in many electromagnetic journals such as *IEEE Antennas and Wireless Propagation Letters*, *IEEE Transaction in Magnetics*, *Progress in Electromagnetic Research*, *European Physical Journal – Applied Physics*, *Journal of Electromagnetic Waves* (JEMW), *Advanced Electromagnetic*, and *International Journal of Microwave and Wireless Technologies*. Dr. Mahmoud was the recipient of Egyptian encouragement state prize award for engineering sciences in 2014. In 2019, he was the recipient of Egyptian El-sherouq innovation award in electronic engineering. He was awarded the top 1% Publon worldwide reviewer award for 2018 and 2019. In 2020, he was named in the top 2% scientists in "A standardized citation metrics author database annotated for scientific field/Updated science-wide author databases of standardized citation indicators".



Mohamed El Atrash received the B.Sc. degree (with honors) in electrical engineering from the Electrical Systems Engineering Department, October University for Modern Sciences and Arts (MSA), Cairo, Egypt, in 2011. He also received the M.Sc. degree (with distinction) in wireless mobile communication system engineering from the University of Greenwich (UoG), UK, in 2014. In 2020, he successfully completed his Ph.D. degree in electrical engineering at Ain Shams University, Cairo, Egypt. His research interests include flexible wearable antennas, high gain, thin, low profile antennas, and EBG/AMC design. Out of his research, he published articles in the *IEEE Transactions on Antennas & Propagation*, *IET Microwaves, Antennas & Propagation*, and the *International Journal of Microwave and Wireless Technologies*, as well as, a number of conference papers. He is a reviewer in the *IET Microwaves, Antennas & Propagation*, since 2019, where he has reviewed more than 15 journals. He also reviewed for *Microwave and Optical Technology*

https://doi.org/10.1017/S1759078721000738 Published online by Cambridge University Press

Letters, *AEUE-International Journal of Electronics and Communications*, and *International Journal of RF and Microwave Computer-Aided Engineering*.



Ahmed A. Abdel Aziz received the B.Sc. degree from Avionics Department (with degree Excellent with honor), Military Technical College, Cairo, Egypt in 2014. He joined the avionics research center from 2014 with the main concern about RF and metamaterial-based components. He received the M.Sc. degree in graphene and metamaterial structures for microwave applications from the Electrical Engineering Department, Military Technical College, Cairo, Egypt in 2019. Ahmed's main concern is microwave components, so he is interested in metamaterials, metasurface, and wearable components.



Mohamed I. Abdelnaser received the B.Sc. degree from Avionics Department (with degree Excellent), Military Technical College, Cairo, Egypt in 2015. He is working in the microwave planning center since 2015. His work is focusing on the development of different microwave and metamaterial-based components and antennas.

https://doi.org/10.1017/S1759078721000738 Published online by Cambridge University Press